Numerical Investigation of Supersonic Flows on Innovative Nozzles (Dual Bell Nozzle)

H. Kbab[†], O. Abada and S. Haif

University of Blida1, Aeronautics and Space Studies Institute, Aeronautical Sciences Laboratory, BP270 Soumaa street, Blida, Algeria

†*Corresponding Author Email: k71.hakim@gmail.com*

ABSTRACT

The Dual Bell Nozzle is the most ambitious of several supersonic, altitude-compensating nozzle concepts for rocket engines. This design's objective is to enhance performance in two different evolving regimes (Sea-Level and High-Altitude Mode) by self-adaptation with no mechanical control. The concept is simple in theory, but the structural efforts involved are significant. The study carried out in this paper is a simulation of the flows in this type of nozzle. Computational fluid dynamics (CFD) is increasingly used as an analytical tool in research and industry. Simulation is not a substitute for experimentation but a complement to it; it allows the analysis of the problem in real conditions (reproduce tests that are done in experimentation to better understand them and at lower cost) or, on the contrary, in extreme or marginal test conditions (extreme climates, installation defects, etc.). Through simulation, the studied system becomes more flexible. We can easily make parametric studies. Simulation almost always takes the form of a program or computer tool. These are commonly called simulation environments. Developments and progress over the past two decades have led to the emergence of a methodology that has become standard. As for any complex system, the control of a phenomenon is based on the identification and modularization of the tasks. Currently, the standard methodology divides the simulation process into four distinct tasks: geometric modeling, meshing, solving, and finally analysis and visualization. In this study, we will present a test case used to validate our computational models that will be used to optimize the profile of a dual bell nozzle. We will use the Ansys-ICEM environment to generate the meshes and the Ansys-Fluent environment to solve the equations of our models. Our results will then be compared with experimental and numerical data from our literature review.

1. INTRODUCTION

The main idea of the dual bell nozzle design is to force the flow to separate from the wall of the nozzle at a predefined inflection point, which improves performance at Sea-Level. This contour inflection provides a controllable and symmetrical detachment of the flow, reducing the generation of significant lateral forces. The flow progressively expands during the climb until it becomes attached to the wall immediately after the inflection point, as seen in Fig. 1.

When the flow is fixed to the wall and the nozzle outlet pressure is higher than the ambient pressure, the performance for the remainder of the climb is enhanced due to the larger effective cross-sections. According to research, this type of nozzle performs similarly to the ideal nozzle, with a maximum area ratio and a margin of error ranging from 1 to 3% (Horn and Fisher 1994). However, the concept has

additional losses of about 3% during low altitude operation due to the aspiration drag due to the non-attachment of the flow on the nozzle extension. Due to the inflection of the contour, these losses are reduced to 0.1–1.2% when compared to a nozzle optimized for the high-altitude mode (Immich and Caporicci 1996; Hagemann *et al.* 1998). As an alternative to profiled nozzles, Foster and Cowles (1949) developed a nozzle with a profile inflection with higher area ratios, which have to support very high side-loads. In the 1990s, experimental and analytical feasibility studies of the dual bell nozzle, such as those by Horn and Fisher (1994) and Hagemann *et al*. (1998), were conducted. Frey and Hagemann (Immich and Caporicci 1996; Fery and Hagemann 1999) estimated that the FSS1 engine can improve payload by up to 72% if a dual bell nozzle is used. Depending on how the launcher was used, Immich and Caporicci (Immich and Caporicci 1997; Fery and Hagemann 1999) predicted a
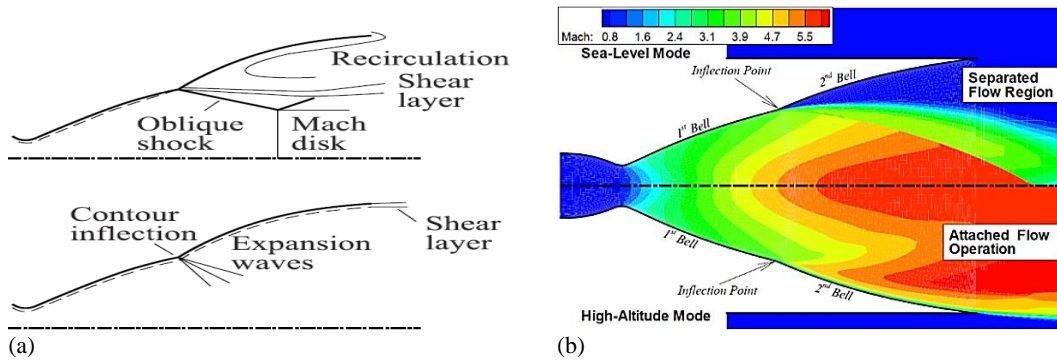
Fig. 1. Operating modes of the dual bell nozzle: (a) (Génin *et al.* 2013), (b) (Martelli *et al.* 2007)

payload increase of up to 33% or 1400 kg. Miyazawa *et al.* (2002) calculated a gain in the specific impulse of 10s. Different types of design concerning the inflexion of the wall and the extension of the basic nozzle have been treated in German analytical and experimental studies (Fery and Hagemann 1999; Martelli *et al.* 2007; Génin and Stark 2009). The dependency of the transition behavior between the two modes (Sea-Level and High-Altitude Mode) received special consideration. Three types of extensions have been tested, namely: TICCP (Truncated Ideal Contour + Constant Pressure extension), TICPP (Truncated Ideal Contour + favorable Pressure gradient) and TICNP (Truncated Ideal Contour + adverse pressure gradient). A TIC (Truncated Ideal Contour) profile was adopted for the first bell (Base Nozzle). The TICNP configuration leads to uncontrolled separation inside the extension, as can be observed in a conventional conical profile or TOC (Thrust-Optimized Contour) nozzle (Hagemann *et al.* 2002; Proschanka *et al.* 2012). On the other hand, the TICCP and TICPP configurations present a faster transition between the two modes: low altitudes and high altitudes (Frey and Hagemann 1999). However, previous experiments with conventional nozzles with adverse pressure gradients have revealed significant side-load problems. Thus, the TICCP configuration was chosen as the most promising for future research. Several experimental, cold gas and hot fire studies and numerical simulations have been carried out to study the TICCP configuration in its two operating modes and the transition between them (Génin and Stark 2007, 2009). Several effects have been analyzed, such as the effect of the divergence angle of the extension (Stark and Génin 2010; Verma *et al.* 2011), the effect of the density of the cold gases (Verma *et al.* 2010), and the effect of the injection of gas at the level of the inflection point on the transition. Due to the effects of viscosity inside the boundary layer, the pressure follows a negative slope and not a discontinuity as predicted by theory. This was described by Martelli *et al.* (2006). The extension must then be divided into the inflection region, where the pressure gradient is negative, and the rest section, where the wall pressure is constant (Stark and Génin 2010). In the same study, Stark and Génin have noticed that before the transition, where the flow quickly recollects on the whole extension, the wall pressure drops in the inflexion region and the point of detachment moves

downstream of the inflexion. This evolution that precedes the real transition is called a "sneak transition." During the ascent, the total pressure remains constant for a real application of a rocket engine. The NPR (Nozzle Pressure Ratio) variation is only due to the variation of the ambient pressure caused by the change in altitude. This variation is very slow, so the "sneak transition" is a critical consideration for the DBN design. This can result in extremely high side loads of the same magnitude as those observed during the ignition and liftoff phases. Verma *et al.* (2013, 2014, 2015) conducted three experimental studies, one of which investigated the influence of the Reynolds number on the transition behavior of a dual bell nozzle during testing within a high-altitude simulation chamber. The second was to examine the effect of ambient pressure changes on transition behavior in a dual bell nozzle. The third study was to execute a cold gas test on a subscale dual bell nozzle operating at Sea-Level to analyze the unsteady flow conditions that occurred during the sneak transition. The last one revealed that the flow during the sneak transition was extremely unsteady and was the main cause of side-load generation. Schneider and Génin (2016) examined the effect of several turbulence models and feed pressure gradients on flow transition behavior in a dual bell nozzle. They concluded that Reynolds stress and the Spalart-Allmaras model produced successful results. Kbab *et al.* (2017) carried out a numerical and simulation study on dual bell nozzles by proposing for the first time a TOP (Thrust Optimized Parabolic) profile for the basic nozzle. Moussa *et al.* (2005) presented a numerical approach to studying the hydrodynamics of a jet generated by supercritical CO_2 fluid expansion through small-diameter nozzles. The main objective of this work concerns the influence of the geometric characteristics of the nozzle on the flow dynamics. The authors noted that the position of the Mach disk and the flow structure are affected not only by the thermodynamic parameters upstream and downstream of the nozzle but also by its geometrical properties.

2. SIMULATION OF FLOWS IN DUAL BELL NOZZLE

In rocket engine applications, nozzles generally have a revolving geometry. In spite of the possible three-dimensional effects likely to develop there,

Table 1 Characteristics of the dual bell nozzle

Quantities	Symbols	Values
Throat radius	R_{th}	10 (mm)
Length of the first curve (bell)	L_b/R_{th}	8.815
Exit radius of the first curve	Y_b/R_{th}	2.885
Length of the second curve	L_{ext}/R_{th}	17.73
Length of divergent	L_{tot}/R_{th}	26.54

the axisymmetric study retains all its interest in the first approach since it allows calculating at a lower cost the majority of the characteristics of this type of flow. In our case, we limit ourselves to the study of the modeling of stationary phenomena. The design of the original geometry was generated by a computational code in FORTRAN using the MOC. Our study's test case is a dual bell nozzle with a TIC first profile. The attachment point has the coordinates Xa and Ya, which are respectively equal to 0.00902117 [m] and 0.01138849 [m]. On the other hand, the junction point between the two curves is defined as Xj = 0.0883 [m], Yj = 0.0286 [m]. The second profile is designed to give a constant wall pressure of P2. The case of inviscid fluids requires that this profile match the isobaric ideal fluid streamline at pressure P2. This is generated by the use of the direct characteristic method for a centering P2/P1 expansion wave that is located at the junction point. The characteristics of our DBN are enumerated in Table 1, and Fig. 2 shows the reproduction of its geometry.

With: R_{th} represent the throat radius.

L_b: Length of the first curve.

Y_b: Exit radius of the first curve.

L_{ext}: Length of the second curve.

L_{tot}: Length of divergent.

2.1 Inviscid Calculation

This first step only concerns the nozzle profile without convergent and without an external domain in inviscid flow. The objective is to verify that the profile obtained does not include any notable shock waves.
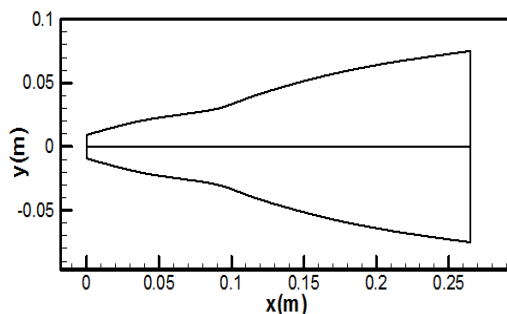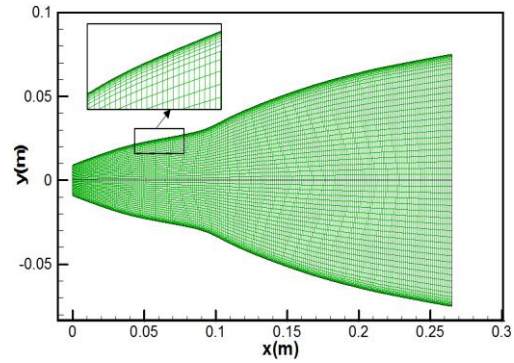

Fig. 3. Structured mesh of the nozzle.

2.1.1 Computational Mesh

Several mesh sizes are used to study the independence of mesh results. These meshes are refined in the throat region and near the wall (regions where the local properties of the flow vary rapidly). Figure 3 shows a monobloc structured mesh of the nozzle geometry generated in the Ansys-ICEM environment. A total of 386 nodes were distributed on the border of the profile. The mesh consists of a total of 11910 quadrilateral cells.

2.1.2 Boundary Condition

Figure 4 summarizes the boundary conditions used in the calculation model. The same boundary conditions will be used in the different test cases by changing the values assigned to the inlet and outlet variables to account for the operating of both Sea-Level Mode and High-Altitude Mode.

Several simulation calculations were performed in an inviscid stationary axisymmetric model. These simulations allowed a first validation of the numerical results against the results of reference (Reijasse *et al*. 2011) to comprehend the sensitivity of this type of flow to predefined boundary conditions. Table 2 represents a summary of the boundary conditions used for the test case in operation in High-Altitude Mode (AM), NPR =806.

With: P_0 represent the Chamber pressure.

T_0: Stagnation temperature.
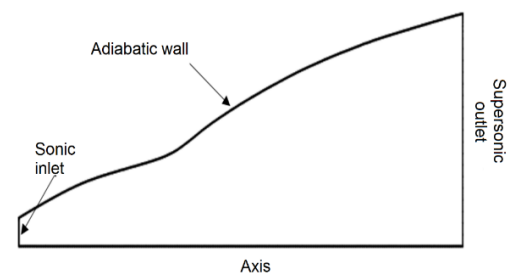
P_S: Static pressure.

T_S: Static temperature.

Fig. 2. Nozzle geometry.

Fig. 4. Boundary Conditions imposed in the model.

Table 2 Boundary conditions of the inviscid model in AM mode.

model	2D, axisymmetric, stationary
Solver	Coupled, implicit
Fluid	Air, ideal gas law
Inlet Boundary Conditions	Inlet Pressure $P_0 = 52 \times 10^5\ Pa$ $P_S = 509980\ Pa$ $T_0 = 330\ K$
Outlet Boundary Conditions	Outlet Pressure $P_S = 6448\ Pa$ $T_S = 48.76\ K$
Walls	Wall (adiabatic wall)

2.1.3 Solution Convergence

To ensure convergence, we impose very strict convergence criteria (i.e. 10^{-12}). However, we stop the calculation when it is estimated that convergence is reached (six orders of magnitude are generally sufficient, i.e. 10^{-6}). The criteria we used are that all residues (continuity equation, momentum, and energy) are less than 10^{-6}. The residuals reach constant values that do not change with the increasing number of iterations.

The calculation results (Mach field in particular and the evolution of pressure on the wall and on the axis) are visualized using the Tecplot visualization software. This tool is very powerful in terms of visualizations of flow variables in the form of a field (contours). It also makes it possible to extract variables, in particular the wall pressure, to visualize the velocity vectors and streamlines.

2.1.4 Mach Contours

Figure 5 shows the Mach field in the nozzle by applying the previously defined boundary conditions (i.e. inviscid Euler calculation) on our model implemented in Fluent. In order to validate our Mach field, Fig. 6 shows the Mach field in the same nozzle obtained by Reijasse *et al.* (2011). It shows that the flow clings entirely to the wall, which indicates that the flow is not detached. We do not see the formation of an internal shock. Note that it is at this pressure ratio (NPR=806) that this nozzle has been optimized. The Iso-Mach contours
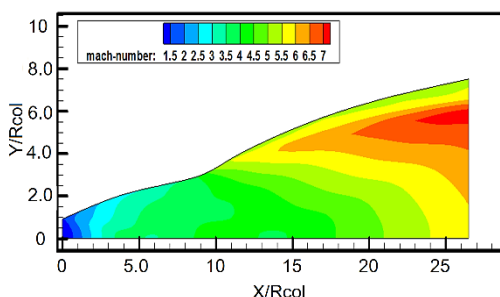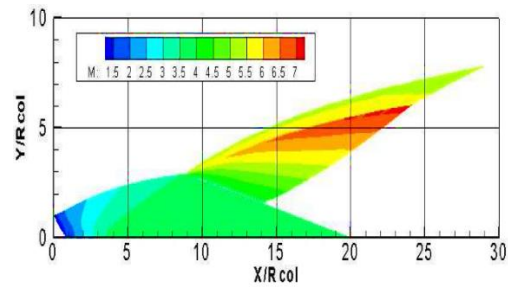

Fig. 6. Iso-Mach contours in the CNES PERSEUS nozzle in AM mode, NPR=806, (Reijasse *et al.* 2011).

of the our dual bell nozzle are very similar to those of (Reijasse *et al.* 2011) which allowed us to judge the good reproduction of the geometry and the good implementation of our model under Fluent (geometry, mesh, boundary condition, and solution methods).

2.1.5 Wall Pressure Coefficient

Wall pressure is a very important parameter in the supersonic flows of the nozzles. Figure 7 represents the evolution of the latter in the nozzle calculated by the characteristic method and the Fluent simulation. We see that the two curves mark an isentropic expansion in the first curve, and at the inflection point (junction between the first and second curve) a drop in pressure is noted. This drop is more pronounced in the case of calculation by MOC, especially as it marks a discontinuity. This is explained by the Prandtl-Meyer expansion fan, which is caused by the sudden deflection of the nozzle profile (angle higher than the angle of Prandtl-Meyer). In the second curve, the two curves mark a horizontal bearing until the nozzle exit.

2.2 Viscous Calculations

Unlike the first step (inviscid calculation), we added a convergent before the throat section and an external domain (very wide) at the nozzle exit. The convergent allowed us to have sonic conditions at
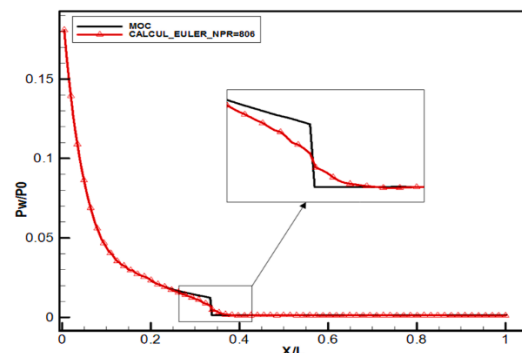

Fig. 5. Iso-Mach contours in the nozzle in AM mode, NPR=806, present study.

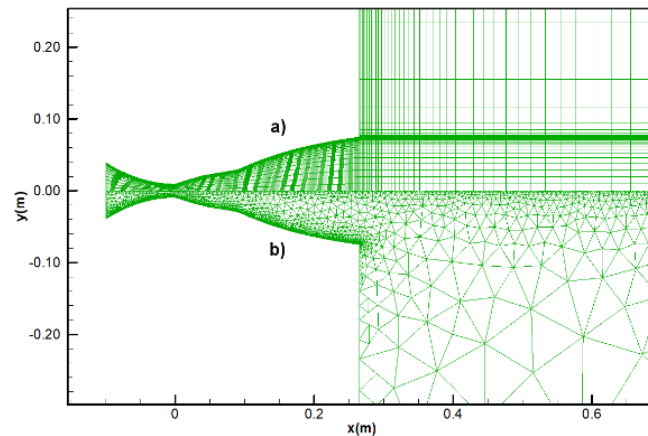**Fig. 7. Comparison between wall pressure calculated by Fluent and by MOC in AM mode, NPR=806.**

Fig. 8. Mesh of the nozzle with convergent and external domain: (a) structured mesh, (b) unstructured mesh.

the throat without resorting to quasi-monodimensional calculation. It was generated using a second degree polynomial to ensure a very low slope to avoid a flow reversal at the inlet. Such a phenomenon generally increases the computation time and especially generates instabilities in computation, such as the divergence of the latter (Denton 2007). The choice of such a model (convergent upstream and external domain downstream) removes several constraints related to the turbulence model and facilitates the choice of boundary conditions. In this case, all that is required is to impose the combustion chamber's stagnation conditions just at inlet and ambient static pressure there at outlet. In other words, we do not have to impose the conditions at the throat or at the nozzle exit, which generally causes results influenced by the type of boundary conditions.

2.2.1 Computational Mesh

Two types of mesh were used, structured and unstructured, both generated in the Ansys-ICEM environment. The purpose of such an approach is to verify the effect of the two meshes on the results as well as the total time invested to perform a calculation. Note that in general, an unstructured mesh is automated, which greatly reduces the model preparation phase. On the other hand, a structured mesh facilitates adaptation (refining cells in areas of interest, e.g. near the wall) without increasing the overall mesh size by a multiplicative factor. Multi-bloc structured mesh with quadrilateral elements has been used to overcome the constraint of unnecessarily refining mesh in areas of lower interest. Figure 8 shows a comparison of the two meshes used. Two blocks have been created in the eternal domain. A fine mesh was generated on the bloc near the nozzle exit. The most downstream block was discretized using a coarsely structured mesh. The general structure of the mesh was maintained for all the test cases. It consists of a total of 171012 cells (quadrilaterals) for the entire model. A total of 300 nodes were distributed on the walls of the divergent nozzle. Most of these nodes were

grouped in the region of the throat and at the junction between the first and second curve (Fig. 8a). A second unstructured mesh was used. The latter consists of 73406 cells (triangular) with a total of 108313 nodes, of which 356 are distributed on the wall nozzle. Note that this mesh has a size of 2.3 which is less than the size of the structured mesh (see below Fig. 8b). The generation of the unstructured mesh was very fast and automatic.

To study the influence of the mesh type on our results, we performed viscous calculations on two structured and unstructured meshes. Calculations are done in AM mode NPR=435 to compare with experimental results. Figure 9 shows the results of calculations compared to the experimental results of (Reijasse *et al.* 2011).

From the figure above, we see that there is no great difference between the results of the two meshes. However, we will use the multi-block structured mesh in the next test cases for the following reasons:

1. The use of an unstructured mesh for turbulent calculation requires refinement near the wall (to ensure a y^+ of order 1), without deforming
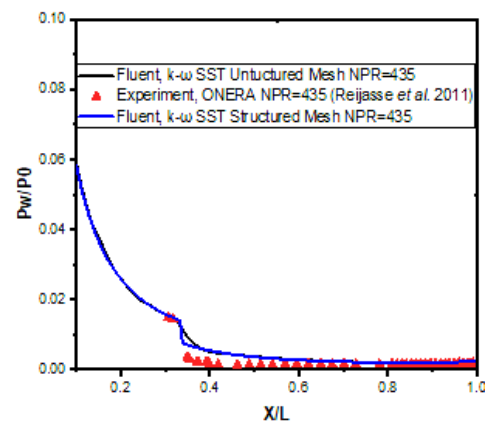

Fig. 9. Comparison of structured and unstructured mesh results for NPR=435.

the triangular cells, which extend the calculation. y^+ represents the dimensionless distance from the first mesh to the wall.

2. We can control the generation of the structured mesh, but not the unstructured.

3. The convergence of computation for an unstructured mesh is more costly in terms of computation time than that of a structured mesh (82.12×104 iterations for the unstructured mesh against 33.4×104 iterations for the structured mesh).

Fig. 10. Mesh in the area near the wall.

2.2.2 Boundary Condition

In order to faithfully reproduce the physics problem, it is important to treat carefully the computational domain's boundary conditions. In the inlet plane (of the convergent), we impose boundary conditions resulting from the stagnation conditions of the combustion chamber. Table 3 shows the different boundary conditions used in this test case.

The outlet conditions of the calculation domain are not shown in Table 3 because several simulations were made by varying the outlet pressure to have all the operating modes of the nozzle pass from the Sea-Level Mode (SM), Transition Mode (TRAN) to High-Altitude (AM) Mode.

2.2.3 Turbulence Model

The numerical method used, specifically the turbulence model, has a significant effect on the accuracy of flow prediction for high Mach number nozzles. Tandra *et al*. (2008) and colleagues created the modified k-ε model for usage and replies to objections leveled against the k-ε model by several authors, who claim that it is unable to correctly predict the average velocity profile of axisymmetric turbulent jets due to the compressibility effect. In several works, the k-ω SST model has provided

Table 3 Boundary conditions of the viscous model.

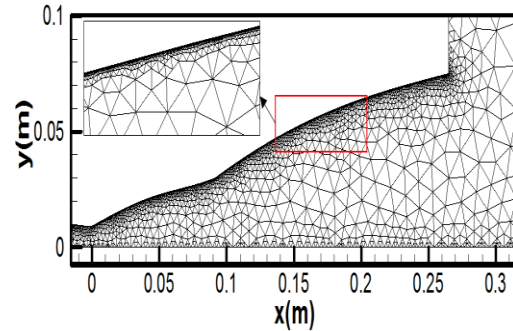| model	2D, axisymmetric, stationary
Solver	Coupled, implicit
Fluid	Air, ideal gas law
turbulence model	k-ω SST
Inlet Boundary Conditions	Inlet Pressure $P_0 = 52 \times 10^5\ Pa$ $P_S = 519980\ Pa$ $T_0 = 330\ K$
Outlet Boundary Conditions	–
walls	Wall (adiabatic wall)

complete satisfaction. For example, in a comparison of the experimental and numerical results of Hunter (2007) using several turbulence models, the k-ω SST model provided the results that were closest to the experimental in terms of prediction of shock waves and their position. Perrot (2006) points out that the k-ω SST model predicts the distribution of wall pressure in very good agreement with experience, and it allows the positioning of the point of detachment in the correct position.

2.2.4 Calculation of y^+

As already pointed out, the Reynolds number is high, and the flow is not laminar at all. That said, we are obliged to use a turbulence model. In contrast to the inviscid case, the solutions are more dependent on the mesh size, and special attention must be focused to checking the mesh size near the walls to ensure that all phenomena are captured. To satisfy the adopted turbulence model (k-ω SST), the first mesh point near wall must be in the viscous sublayer. For this, y^+ must keep a value around 1 near the wall. Figure 10 shows a zoom on the mesh (unstructured) near the nozzle wall. The y^+ is of the order of $0.1 < y^+ < 0.93$ for the structured mesh and of the order of $1.3 < y^+ < 4$ for the unstructured mesh.

2.2.5 Mach contours

The Mach contours in Fig. 11 show the flow development in the nozzle as calculated by a viscous computation with the k-ω SST turbulence model. Figure 11(a) shows operation in AM mode, NPR=435 and Fig. 11(b) shows operation in SM mode, NPR=80. AM mode contours are computed on a structured mesh and SM mode contours are computed on an unstructured mesh (this choice is discussed below).

In SM mode, where NPR = 80, there is just the first curve, which is in "full flowing" operation. At the inflection point, the flow detaches and creates a free jet inside the second curve. The flow completely adheres to the second curve's nozzle wall in AM mode, when NPR equal 435 (no detachment over the entire length of the extension). This attests to the good implementation of our calculation model under Fluent. A very interesting remark is that the
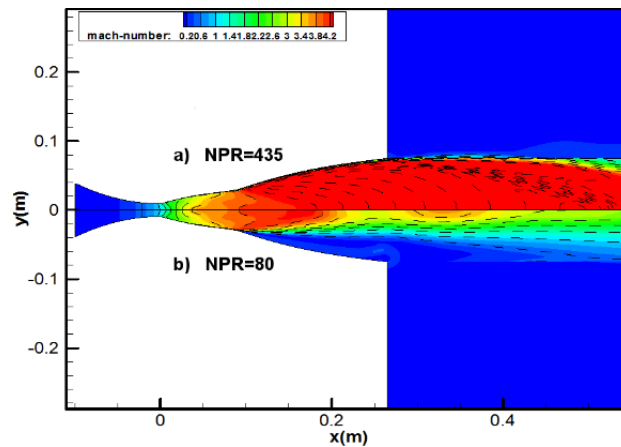
Fig. 11. Iso-Mach contours: (a) in AM mode, (b) in SM mode.

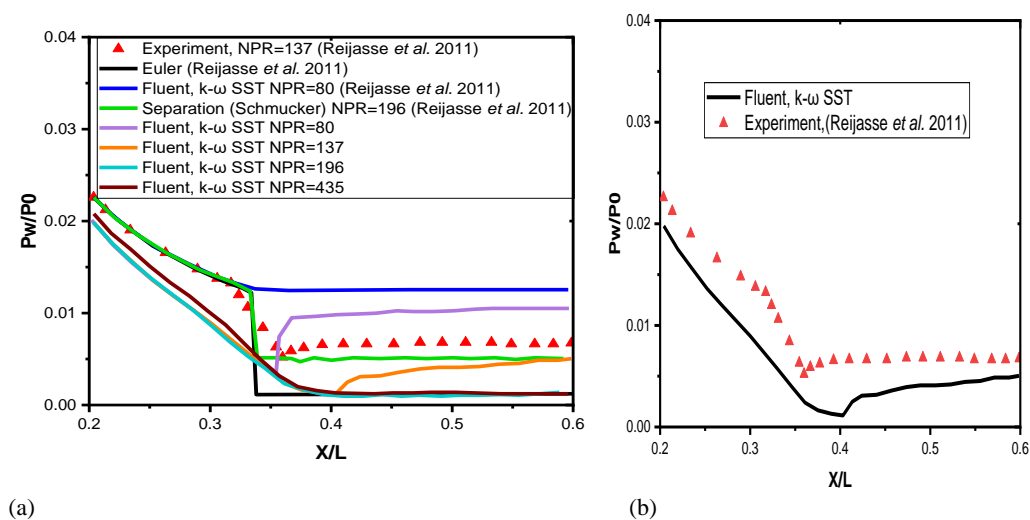(a)   (b)

Fig. 12. (a) Different wall pressure calculated by Fluent compared to those of (Reijasse *et al.* 2011), (b) wall pressure for NPR=137.

operation of the first curve is identical in the two modes, AM; Fig. 11(a) and SM; Fig. 11(b) and this on two different meshes. An additional remark, compared to the inviscid case, is that the boundary layer separation is detected, which reflects more of the physics of the phenomenon. These remarks allow us to say that the implementation of our model, including the turbulence model, has been successful.

2.2.6 Wall Pressure Coefficient

Figure 12 (a) shows the various wall pressure evolutions in the divergent as estimated using the Fluent k-ω SST turbulence model. The parameter values obtained are compared with the numerical and experimental results obtained by (Reijasse *et al.* 2011). Figure 12(b), for improved comparison with experimental results, shows the evolution of the same parameter for an NPR of 137.

Analyzing Fig. 12, we find a very good consistency

between our results and those of (Reijasse *et al.* 2011). This is true for numerical and also experiments conducted. For all NPR less than 137, the nozzle operates in SM mode. It is clearly demonstrated by the wall pressure increase just below the inflection point. It operates in transient mode (TRAN) for NPR=137. In this mode (TRAN) we detect that the point of separation is slightly downstream compared to what was detected experimentally. The application of the Schmucker criterion (Schmucker 1984) carried out by (Reijasse *et al.* 2011) to detect boundary layer detachment at NPR equal 196 gives in a slightly greater wall pressure than our results using the k-ω SST model. For NPR values greater than or equal to 196, the nozzle functions in AM mode. Figure 13 shows the Mach field for transient mode operation. A zoom is made in the recirculation zone (by visualizing the velocity vectors) to facilitate interpretation. Contrary to the case of the SM mode where the point of separation was fixed on the point of inflection, the point of separation in transient mode is pushed back downstream on the extension wall.
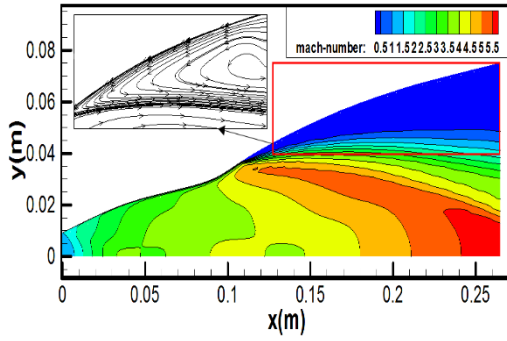
Fig. 13. Iso-Mach contours in the CNES PERSEUS nozzle in TRAN mode, NPR=137.

2.3 Altitude Adaptation

To study the altitude adaptation of the nozzle, we varied the static pressure outside the nozzle, and then we visualized the structure of the flow inside and outside of the nozzle. The stagnation conditions are; P0 = 10 atm, T0=243 K. Different simulations of the Iso-Mach for different NPR are shown in Fig. 14–21.
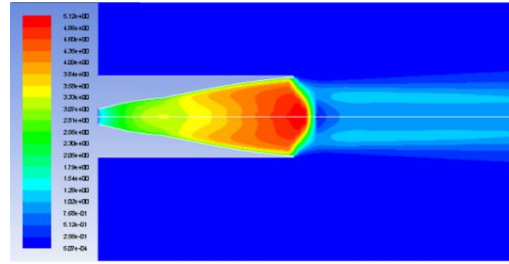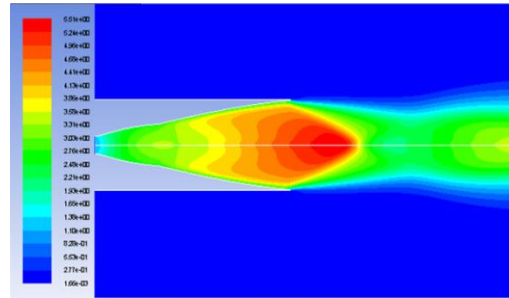

Fig. 14. Mach number contours for NPR=9.89.
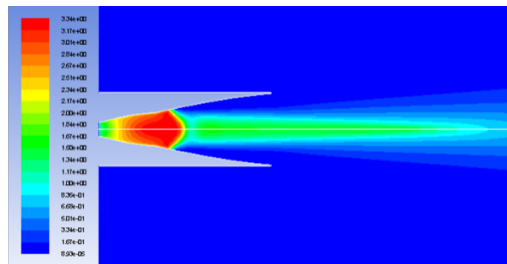

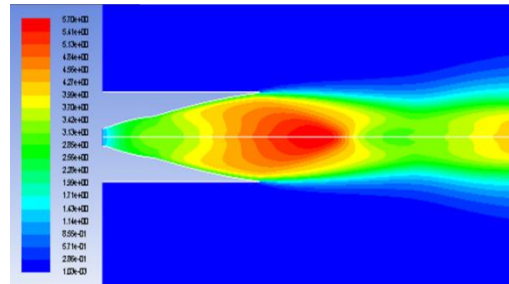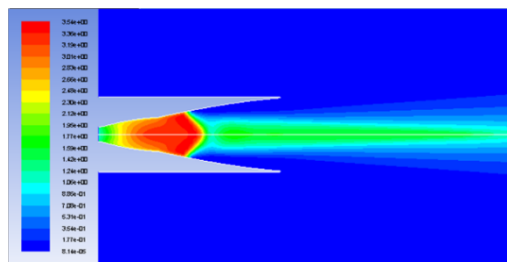**Fig. 15. Mach number contours for NPR=12.5.**

Fig. 16. Mach number contours for NPR=20.

Fig. 17. Mach number contours for NPR=28.57.

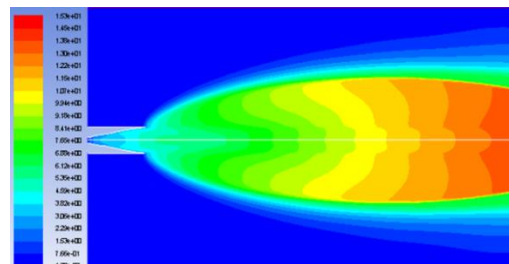**Fig. 18. Mach number contours for NPR=98.69.**

Fig. 19. Mach number contours for NPR=200.
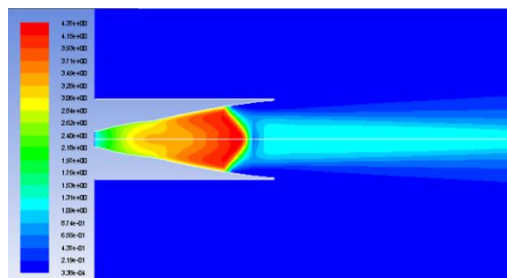

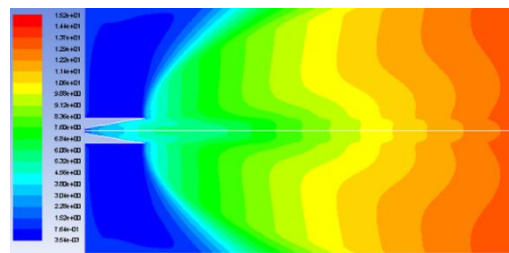**Fig. 20. Mach number contours for NPR=10000.**

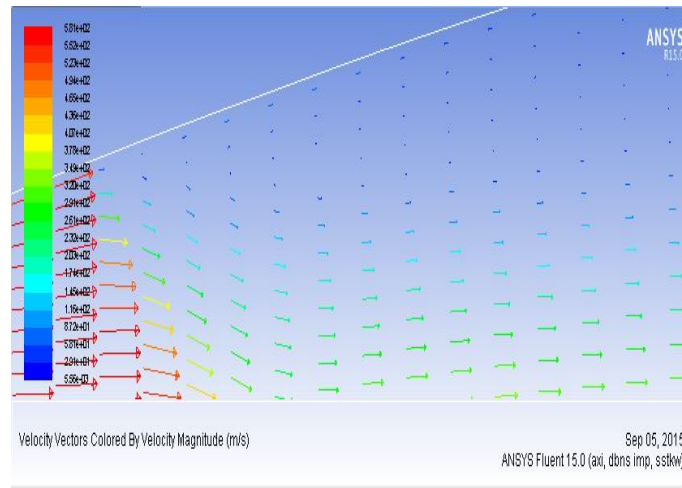**Fig. 21. Mach number contours for NPR=1000000.**

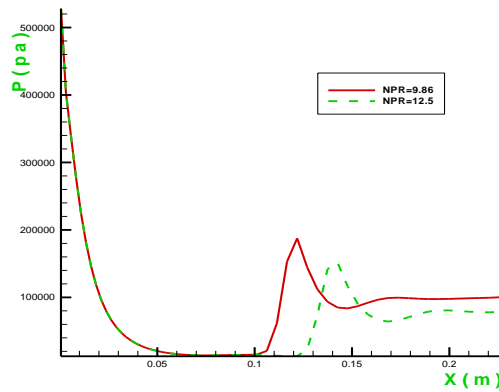**Fig. 22. Boundary layer separation for NPR=9.86.**

Fig. 23. The position of the shock wave for different pressure ratio.

For NPR = 9.86, we note the appearance of shock waves inside the nozzle, and the flow downstream of the shock wave separates from the wall since the downstream pressure is very high (overexpansion regime). The fluid outside the boundary layer has enough movement to overcome the adverse pressure gradient that tries to push the fluid backwards. The fluid in the boundary layer has a low momentum, which is due to the friction between the fluid and the solid wall, and therefore the fluid will not be able to counteract the adverse pressure gradient and will be quickly brought to a stop and possibly reverse its direction. If this reversal occurs, the boundary layer detaches from the solid wall see Fig. 22. When the NPR is increased to 12.5, the flow expands further, and the position of the shock wave and the separation point move downstream of nozzle, but the flow remains overexpanded (Fig. 23).

By further increasing the NPR to reach 28.57, the nozzle works optimally since there is no shock wave inside the nozzle and the flow continues to expand optimally outside the nozzle. By setting the NPR to 200, an under expansion appears since the nozzle exit pressure is higher than the ambient pressure Then, a succession of expansion waves occur as the gases continue to expand outside the nozzle. Finally, for a NPR=1000000, the flow is characterized by a strong under expansion because the ambient pressure is too low. This induces severe turbulence, which results in a highly unstable flow, a shock wave starts outside the nozzle. This indicates that for a certain mass flow, this ambient pressure is too low to be used for this nozzle.

3. CONCLUSION

This paper proposes a study to simulate flows in dual bell nozzles. The characteristics method is used to create the design. The base nozzle is considered as a TIC profile. On the other hand, the second curve's profile is determined to generate a constant wall pressure P2. The case of inviscid fluid requires that this profile match the isobaric ideal fluid streamline at pressure P2. This is generated by the use of the direct characteristic method for a centering P2/P1 expansion wave that is located at the junction point. The simulation was done in both viscous and inviscid cases.

1. Mesh sensitivity was tested using multiple sizes to study the independence of mesh results.

2. The choice of unstructured mesh was well justified and argued.

3. The k-ω SST turbulence model is the most suitable model for simulating flow in the nozzles.

The results obtained in the study are very satisfactory. The flow logic in the dual bell nozzles was respected in all cases. The comparison of our results with those obtained by other authors was satisfactory. As an alternative, we propose expanding this research to include experimental tests to definitively validate such an approach. In the aerothermal field, it would be interesting to develop models that take into account the thermal

aspects in addition to the turbulence, so the study of the side-loads exerted on the nozzle, particularly at the inflection point, is necessary. Finally, it is very interesting to investigate the evolution of the flow parameters using the TVD (total variation diminishing) scheme, which was developed specifically to obtain oscillation-free solutions (Yee *et al.* 1985).

REFERENCES

Denton, B. L. (2007). *Design and Analysis of Rocket Nozzle Contours for Launching Pico-Satellites*. M. Sc. thesis, Mechanical Engineering (KGCOE), Rochester, USA.

Foster, C. and F. Cowles (1949). Experimental study of gas-flow separation in overexpanded exhaust nozzles for rocket motors (No. JPL-PR-4-103).

Frey, M. and G. Hagemann (1999). Critical assessment of dual-bell nozzles. *Journal of Propulsion and Power* 15(1), 137-143.

Génin, C. and R. Stark (2007, January). Experimental study of dual-bell nozzle. In *2nd European Conference for Aerospace Science (EUCASS)*, Bruxelles, Belgium.

Génin, C. and R. Stark (2009). Flow Transition in dual-bell nozzles. *Shock Waves* 19(3), 265-270.

Génin, C., R. Stark, O. Haidn, K. Quering and M. Frey (2013). Experimental and numerical study of dual-bell nozzle flow. *Progress in Flight Physics* 5, 363-376.

Hagemann, G., H. Immich, T. V. Nguyen and G. E. Dumnov (1998). Advanced rocket nozzles. *Journal of Propulsion and Power* 14(5), 620-634.

Hagemann, G., M. Terhardt, D. Haeseler and M. Frey (2002). Experimental and analytical design verification of the dual-bell concept. *Journal of Propulsion and Power* 18(1), 116-122.

Horn, M. and S. Fisher (1994). Dual-bell altitude compensating nozzles. *NASA Propulsion Engineering Research Center* 2.

Hunter, C. A. (2007, July). Experimental, theoretical and computational investigation of separated nozzle flows. In *34th AIAA/ASME/SAE/ASEE Joint propulsion conference*, Cleveland, OH, USA.

Immich, H. and M. Caporicci (1997, July). Status of the FESTIP rocket propulsion technology program. In *33rd AIAA Joint Propulsion Conference*, Seattle, WA, USA.

Immich, H. and M. Caporicci (1996, July). FESTIP technology developments in liquid rocket propulsion for reusable launch vehicles. In *32nd AIAA Joint Propulsion Conference*, Lake Buena Vista, Florida, USA.

Kbab, H., M. Sellam, T. Hamitouche, S. Bergheul and L. Lagab (2017). Design and performance evaluation of a dual bell nozzle. *Acta Astronautica* 130, 52-59.

Martelli, E., F. Nasuti and M. Onofri (2006, July). Thermo-fluid dynamics analysis of film cooling in over expanded rocket nozzles. In *42nd AIAA Joint Propulsion Conference*, Sacramento, CA, USA.

Martelli, E., N. Francesco and M. Onofri (2007). Numerical parametric analysis of dual-bell nozzle flows. *AIAA Journal* 45(3), 640-650.

Miyazawa, M., S. Takeuchi and M. Takahashi (2002, January). Flight performance of dual-bell nozzles. In *40th Aerospace Science Meeting*, Reno, NV, USA.

Moussa, A. B., H. Ksibi, C. Tenaud and M. Baccar (2005). Paramètres géométriques de contrôle de la détente d'un fluide supercritique. *International Journal of Thermal Sciences* 44(8), 774-786.

Perrot, Y. (2006). *Étude, Mise au Point et Validation des Modèles de Turbulence Compressible*. Ph. D. thesis, Université de Rouen, France.

Proschanka, D., K. Yonezawa, H. Koga, Y. Tsujimoto, T. Kimura and K. Yokota (2012, May). Control of operation mode transition in dual-bell nozzles with film cooling. In *46th AIAA/ASME/SAE/ASEE Joint Propulsion Conference*, Nashville, TN, USA.

Reijasse, P., D. Coponet, J. M. Luyssen, V. Bar, S. Palerm, J. Oswald, F. Amouroux, J. C. Robinet and P. Kuszla (2011). Wall pressure and thrust of a dual-bell nozzle in a cold gas facility. *Progress in Propulsion Physics* 2, 655-674.

Schmucker, R. H. (1984). Flow processes in overexpanded chemical rocket nozzles. Part 1: Flow separation (No. NASA-TM-77396).

Schneider, D. and C. Genin (2016). Numerical investigation of flow transition behavior in cold flow dual-bell rocket nozzles. *Journal Propulsion Power* 32(5), 1212-1219.

Stark, R. and C. Génin (2010, July). Side loads in dual-bell nozzles, Part I Phenomenology. In *46th AIAA Joint Propulsion Conference,* Nashville, TN, USA.

Tandra, D., A. Kaliazine, D. E. Cormack and H. N. Tran (2006). Numerical simulation of supersonic jet flow using a modified k− ε model. *International Journal of Computational Fluid Dynamics* 20(1), 19-27.

Verma, S. B., A. Hadjadj and O. Haidn (2015). Unsteady flow conditions during dual-bell sneak transition. *Journal Propulsion Power* 31(4), 1175-1183.

Verma, S. B., R. Stark, C. Genin and O. Haidn (2010). Cold-gas experiments to study the flow separation characteristics of a dual-bell nozzle

during its transition modes. *Shock Waves* 20(3), 191-203.

Verma, S. B., R. Stark and O. Haidn (2013). Reynolds number influence on dual-bell transition phenomena. *Journal Propulsion Power* 29(3), 602-609.

Verma, S. B., R. Stark and O. Haidn (2014). Effect of ambient pressure fluctuations on dual-bell transition behavior. *Journal Propulsion Power*

30(5), 1192-1198.

Verma, S. B., R. Stark, C. Génin and O. Haidn (2011). Cold gas dual-bell tests in high-altitude simulation chamber. *Shock Waves* 21(2), 131-140.

Yee, H., R. Warming and A. Harten (1985). Implicit total variation diminishing (TVD) schemes for steady-state calculations. *Journal of Computational Physics* 57(3), 327-360.